Nanoscale

PAPER

Metalation of tetraphenylporphyrin with nickel on a TiO₂(110)-1×2 surface†

Cici Wang,‡[a] Qitang Fan,‡[a] Yong Han,[a] José I. Martínez,[b] José A. Martín-Gago,[b] Weijia Wang,[a] Huanxin Ju,[a] J. Michael Gottfried[* c] and Junfa Zhu[* a]

The *in-situ* metalation of tetraphenylporphyrin (2HTPP) with Ni on the reconstructed TiO₂(110)-1×2 surface, resulting in the formation of adsorbed nickel(II)-tetraphenylporphyrin (NiTPP), has been investigated by synchrotron radiation photoemission spectroscopy (SRPES), scanning tunnelling microscopy (STM) and *ab initio* Density Functional Theory (DFT) calculations. The metalation can be realized at room temperature irrespective of the deposition order of Ni and 2HTPP, which however leads to different metalation degrees. Increasing the substrate temperature or Ni:2HTPP ratio results higher metalation degree, which ultimately reaches its limit at ~85% (Ni:2HTPP = 3:1) and ~49% (Ni:2HTPP = 1:1) for the cases of post- and pre-deposition of Ni, respectively. The reaction from 2HTPP to NiTPP is accompanied by changes of the molecular adsorption conformation and the adsorption sites from tilted two-lobed on added Ti₂O₃ rows to a four-lobed feature on top of troughs or cross-links of the TiO₂(110)-1×2 surface. This interpretation of the STM data is supported by DFT-based STM simulations.

Introduction

Metalloporphyrins at surfaces and interfaces[1,2] have been extensively studied due to their important applications as building blocks for the design of supramolecular architectures,[3-5] spintronics,[6] in gas sensors[7-12] and as catalysts.[13-15] It has been shown that metalloporphyrins can be synthesized by incorporation of metal atoms into adsorbed free-base porphyrin molecules under ultrahigh-vacuum (UHV) conditions.[16] This metalation process is a redox reaction, resulting in the oxidation of the metal and a reduction of the porphyrin ligand.[17] Examples include the reactions of tetraphenylporphyrin (2HTPP) with post- or pre-deposited metals, such as Fe, Co, Ni, Cu, Zn and Ce,[16-27] or directly with the substrate atoms.[28-33] The conditions under which metalation occurs depend on the type of the metal. As reported previously, the metalation has substantial activation barriers for Zn and Cu, but less so for Fe, Co and Ni, resulting in different degrees of metalation achievable at room temperature.[17] Elevating the substrate temperature generally results in further metalation by overcoming the metalation activation barrier.[19, 24] However, even at sufficiently high temperature and with an excess of the reactant metal, the degree of metalation varies with the substrate, indicating a pronounced additional influence adsorbate-substrate interactions, which can affect both the porphyrin and the co-adsorbed metal.[19, 24, 26]

It has been proposed that adsorbed metal atoms and molecules can diffuse toward each other before the molecular centers coordinate and subsequently react with metal atoms.[26] High degrees of 2HTPP metalation were usually obtained on coinage metal surfaces due to their high diffusion rates of both 2HTPP and metal atoms.[19]

Recently, we have studied an interesting system of 2HTPP on a semiconductor TiO₂ surface.[34] Metalloporphyrins and complex porphyrin arrays bound to TiO₂ have attracted widespread attention because they are promising candidates for efficient photovoltaic applications due to the close match of their photoabsorption to the solar spectrum.[35-38] In addition, CoTPP supported on TiO₂ is an effective catalyst for the reduction of NOₓ with H₂ or CO[39, 40] and the photocatalytic degradation of dyes.[14, 15, 41, 42] It has been demonstrated that the metalation of 2HTPP with Ni can be achieved on a rutile TiO₂(110)-1×1 surface,[34] however, the maximum metalation degree is lower (~60%) than on metal surfaces.[19, 26] This finding was attributed to the formation of large stable Ni clusters and the low mobility of Ni atoms and 2HTPP on the relatively corrugated TiO₂(110)-1×1 surface. In addition, the maximum degree of metalation achieved was almost independent of the deposition order of Ni and 2HTPP on the TiO₂(110)-1×1 surface, similar to related findings for metalation on metal surfaces.[19]

To obtain complementary insight into our previous work on TiO₂(110)-1×1 we have selected the even more corrugated and reduced TiO₂(110)-1×2 surface as a substrate to study the metalation of (sub)monolayer coverages of 2HTPP with Ni atoms using techniques including synchrotron radiation based photoelectron spectroscopy (SRPES) and scanning tunnelling microscopy (STM) under ultrahigh vacuum (UHV) conditions. The rutile TiO₂(110)-1×2 surface can be prepared with large terraces through reducing the TiO₂(110)-1×1 surface and thus serve as a model surface for fundamental research.[43] Differences in the interaction of Ni

[a.] National Synchrotron Radiation Laboratory and Collaborative Innovation Center of Suzhou Nano Science and Technology, University of Science and Technology of China, Hefei, 230029, P. R. China. E-mail: jfzhu@ustc.edu.cn
[b.] ESISNA Group, Dept. Surfaces, Coatings and Molecular Astrophysics, Institute of Material Science of Madrid (ICMM-CSIC), Sor Juana Inés de la Cruz, 3, 28049, Madrid, Spain.
[c.] Fachbereich Chemie, Philipps-Universität Marburg, Hans-Meerwein-Str. 4, 35032, Marburg, Germany. E-mail: michael.gottfried@chemie.uni-marburg.de
† Electronic supplementary information (ESI) available: [Valence band spectra, DFT, STM images and histograms]. See DOI: 10.1039/x0xx00000x
‡ These two authors contributed equally to this paper, and share first authorship.

2HTPP with the two TiO_2 surfaces, $TiO_2(110)$-1×2 and $TiO_2(110)$-1×1, are expected to affect the metalation process and in particular the maximum degree of metalation.
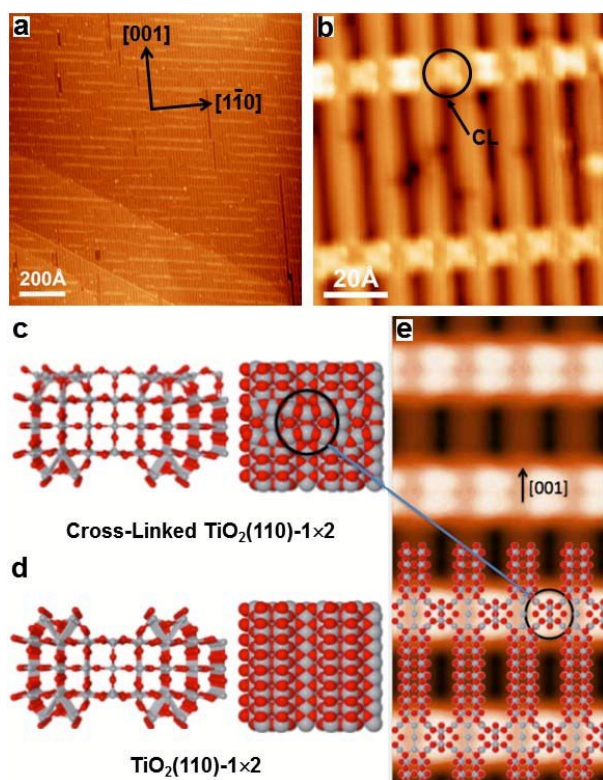
Experimental and Computational Details

The experiments were performed in two separate ultrahigh vacuum systems. The SRPES experiments were performed at the 10D beamline in the Pohang Light Source (PLS), Korea. A photon energy of 550 eV was used to probe the N 1s core level. Valence band spectra were recorded with a photon energy of 55 eV. All binding energies (BEs) were referenced to Au $4f_{7/2}$ (BE = 84 eV) which was measured after each spectrum using an Au foil fixed below the sample. The deconvolution (fitting) of the XP spectra was performed using the XPSPeak program with Gaussian–Lorentzian functions after subtracting a Shirley background. During each N 1s spectrum fitting procedure, the intensity ratio of the two nitrogen components (pyrrolic (-NH-) and iminic (=N-)), binding energy and full width at half maximum (FWHM) were fixed. The STM experiments were carried out in a SPECS STM 150 Aarhus with SPECS 260 electronics. All given voltages were applied to the sample and the images were taken in constant-current mode using a tungsten tip. The STM images were processed with the WSxM software.[44] Measurements of cluster

Fig. 1 (a) Overview STM image of the clean $TiO_2(110)$-1×2 surface; (b) Magnified view of $TiO_2(110)$-1×2 showing the cross-links (CLs, black arrow), which are labelled by black circles. Tunnelling parameters: I = 0.10 nA, U = 2.2 V in all cases; (c, d) Side and top view of structural (optimized) models of the cross-linked and the conventional $TiO_2(110)$-1×2 surface. The gray and red spheres represent Ti and O atoms, respectively; (e) Simulated STM image with the tunnelling parameters of panel b.

heights from STM images were conducted with a commercial SPIP analysis program.

A one-side polished rutile $TiO_2(110)$ sample was cleaned by several cycles of Ar^+ sputtering followed by annealing at about 1100 K in UHV. After several cycles, TiO_2 was reduced and sufficiently conductive for XPS and STM experiments. The cleanliness and order of the surface were confirmed by a combination of SRPES, STM, and low energy electron diffraction (LEED). 2HTPP and NiTPP (purity > 98%, Porphyrin Systems GbR) were degassed in vacuo at 450 K for 24 h. Ni (purity > 99.999%) was evaporated from a wire filament. The thicknesses of the layers were estimated with a quartz crystal microbalance. The 2HTPP or NiTPP monolayers and submonolayers were prepared by vapor deposition onto the $TiO_2(110)$ substrate held at 300 K. All photoemission spectra and STM images were obtained at room temperature. The coverage θ of the molecules on the TiO_2 substrate was defined as the number of adsorbed molecules per $TiO_2(110)$-1×2 surface unit cell. A complete layer of porphyrin molecules on $TiO_2(110)$-1×2 corresponds to $\theta = 0.197$. The actual coverage in the experiments was determined by STM investigation.

In order to shed light on the structural, electronic and STM properties of the (2H/Ni)TPP molecules deposited on $TiO_2(110)$-1×1 and $TiO_2(110)$-1×2 surfaces we have carried out first-principles DFT-based calculations. For this purpose we have combined the localized basis-set and plane-wave DFT-schemes as implemented in the FIREBALL[45] and QUANTUM ESPRESSO[46] simulation packages, respectively. In the latter, an efficient perturbative van der Waals (vdW) correction was implemented.[47] Additionally, tunnelling currents for the STM images were calculated by using a Keldysh–Green function formalism, together with the first-principles tight-binding Hamiltonian obtained using the local-orbital DFT-FIREBALL method.[45, 48] Given the large amount of atoms involved in all the calculations, we have limited the depth of the substrate slabs mimicking the TiO_2 surfaces to five oxide physical layers for the $TiO_2(110)$-1×1 phase and four oxide physical layers for the $TiO_2(110)$-1×2 phase, keeping fix in the relaxations the two bottommost layers. The relevance of sufficiently thick slabs for obtaining accurate results has been thoroughly analysed in the previous literature.[49] To exclude the presence of artefacts arising from the limited thickness of the slabs, additional calculations were performed in which an extra physical oxide layer was included for both TiO_2 surface reconstructions. These calculations did not reveal any significant variations in the adsorption energies (with an estimated uncertainty of 0.01 eV) or in the electronic structure of the topmost layers with the thickness of the slabs. A more detailed explanation of the theoretical methods and the models used in the calculations can be found in the ESI†.

Results and Discussion

Structure of clean $TiO_2(110)$-1×2

The rutile $TiO_2(110)$ surface forms several reconstructions depending on its degree of reduction. The freshly prepared TiO_2 sample adopts a 1×1 structure. Further reduction leads to its reconstruction from 1×1 to 1×2 and cross-linked 1×2 surface. After several sputtering and annealing cycles, a $TiO_2(110)$-1×2 surface with large terraces was achieved, as displayed in Fig. 1a. Based on STM observations and

first-principles calculations, the two most debated structures proposed for the 1×2 reconstruction are the added-row structures Ti_2O_3[50, 51, 52] and Ti_2O[53, 54]. More recent studies have demonstrated that Ti_2O_3-added row is the most reasonable structure. In particular, Elliott *et al.* showed that the simulated STM image of the Ti_2O_3 added-row structure agreed the best with the experimentally observed STM image.[55] Ünal *et al.* proposed that the Ti_2O_3 structure is more stable than the Ti_2O structure on the basis of DFT+U calculations.[56] The Ti_2O_3 added row appears as bright stripes along the [001] direction, as shown in Fig. 1b.[43] The bright contrast of the long stripes arises from the Ti atoms inside the Ti_2O_3 rows. The additional extra brilliant stripes extending along the [1$\bar{1}$0] direction in Fig. 1b are known as cross-links (CL, marked with black arrows). Fig. 1c shows the side and top view of the calculated structure of the cross-links, which have been reported to consist of single Ti_2O_3 moieties trapped at the surface troughs between the long stripes.[57] For comparison, Fig. 1d shows the calculated structure of the 1×2 reconstruction without CLs. A simulated STM image of the cross-linked TiO_2(110)-1×2 surface, partially overlaid with a structural model, is shown in Fig. 1e. As marked by black circle, six coordinatively unsaturated Ti atoms are included in a single cross-link.[58]

Metalation of (sub)monolayer of 2HTPP

Fig. 2a shows the N 1s spectrum of a monolayer 2HTPP on TiO_2(110)-1×2, which contains two non-equivalent nitrogen species,

pyrrolic (-NH-, 400.1 eV) and iminic (=N-, 397.9 eV) nitrogen atoms, in agreement with previous literature.[19, 24, 32, 34] Despite the formal 1:1 stoichiometry in the pure 2HTPP, the -NH- related peak is larger than the -N= related peak by ~50%. This frequently observed deviation from the ideal stoichiometry has been attributed to photoelectron diffraction,[28] however, we cannot entirely exclude partial hydrogenation of -N=, for example through reaction with hypothetical residual hydroxyl. After post-deposition of a stoichiometric amount of nickel onto the 2HTPP monolayer, the two 2HTPP related N 1s peak lose their intensities and a new peak appears at 398.8 eV, as shown in Fig. 2b (green line). The binding energy (BE) of this new peak is identical to the reference spectrum in Fig. 2f, which was obtained from a monolayer of pure NiTPP on TiO_2(110)-1×2. Therefore, the new peak is assigned to N atoms in NiTPP formed by the metalation of 2HTPP with Ni. This conclusion is further supported by the valence band spectra shown in Fig. S1 (ESI†). The corresponding yield of NiTPP is ~27% of the initial 2HTPP, as determined by comparing the integrated areas for all components in the N 1s XP spectrum in Fig. 2b. This value is lower than the metalation degree obtained on TiO_2(110)-1×1 (~35%) under
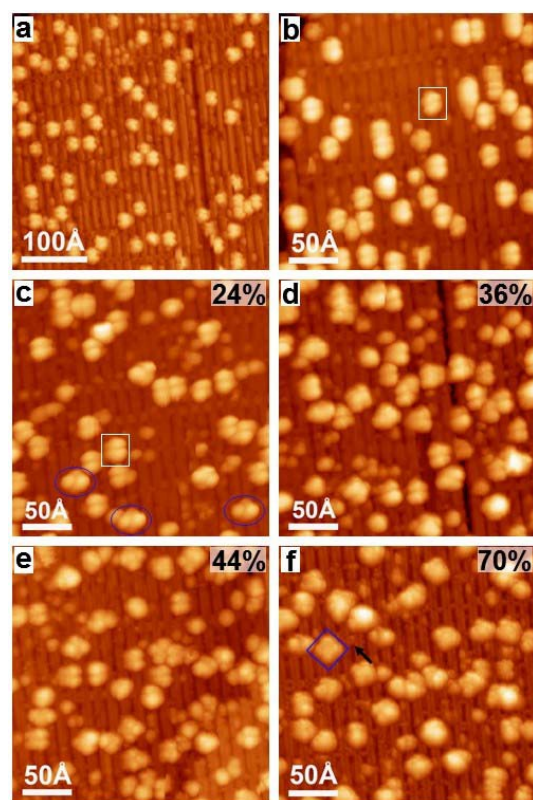
Fig. 3 STM images taken after (a) deposition of a 2HTPP submonolayer ($θ_{2HTPP}$ = 0.02) on TiO_2(110)-1×2 and (b) a magnified view of the sample in (a), one 2HTPP molecule is labelled by a white rectangle; (c-e) incremental deposition of Ni onto 2HTPP with Ni:2HTPP ratios of 1:1, 2:1 and 3:1; (f) heating sample (e) to 550 K. Three types of molecules are labelled by white rectangle, blue oval and square (see the text). The black arrow pointed a CL. Tunnelling parameters: (a) I = 0.04 nA; (b) I = 0.02 nA; (c) I = 0.04 nA; (d) I = 0.05 nA; (e) I = 0.06 nA; (f) I = 0.02 nA. The sample bias voltage was - 2.2 V in all cases. The average metalation degrees (error ± 8%) of 2HTPP are shown on the upper right corners of the panel c-f.

Fig. 2 N 1s XP spectra (a) of a complete monolayer of 2HTPP on TiO_2(110)-1×2 ($θ_{2HTPP}$ = 0.197) and (b-d) taken after incremental deposition of Ni with Ni:2HTPP ratios of 1:1, 2:1, 3:1 onto the sample (a) at 300 K, (e) after heating sample (d) to 550 K. (f) N 1s XP spectrum of a monolayer of NiTPP on TiO_2(110)-1×2 for comparison. The photon energy was 550 eV. The metalation degree (with error range of ± 5%) of 2HTPP is given for spectra b-e.

otherwise identical conditions.[34] One possible reason for this difference is that both the Ni atoms and the adsorbed 2HTPP molecules have lower diffusion rates on the more corrugated $TiO_2(110)$-1×2 surface, which to some extent hinders the coordination reaction between them. Further increasing the amount of post-deposited Ni to Ni:2HTPP ratios of 2:1 and 3:1 leads to increased amounts of NiTPP, as shown by the intensity growth of the NiTPP related N 1s signal in Fig. 2c and 2d. Upon heating the sample in Fig. 2d to 550 K, the degree of metalation increases from ~66% up to ~85% (Fig. 2e), which is in contrast to the related findings on $TiO_2(110)$-1×1, where no further metalation after annealing to 550 K was observed.[34] This is most possibly due to a higher density of smaller Ni clusters on $TiO_2(110)$-1×2 as compared to $TiO_2(110)$-1×1 at the same Ni coverages.[59] The smaller clusters have higher surface energies and thus higher 2D equilibrium vapor pressures, which facilitates the formation of reactive Ni adatoms.

To further investigate the details of the metalation process, corresponding STM experiments were carried out with a submonolayer of 2HTPP on $TiO_2(110)$-1×2. Fig. 3a shows the STM image taken after deposition of a 2HTPP submonolayer ($\theta_{2HTPP} = 0.02$) on $TiO_2(110)$-1×2 at 300 K. According to the corresponding XP

spectrum, the 2HTPP molecules remain intact on the surface. These intact molecules adsorb on the Ti_2O_3-added rows along the [001] direction and appear as two-lobed features; one example is marked with the white rectangle in Fig. 3b. It has been reported previously that 2HTPP adsorbs on metal or $TiO_2(110)$-1×1 surfaces with a typical two-fold symmetric saddle-shaped conformation.[34, 60] For the here investigated case of 2HTPP on $TiO_2(110)$-1×2, we measured a distance of ~10 Å between two lobes of a single 2HTPP molecule. This value agrees well with the distance between two adjacent (not diagonal!) phenyl legs along the [001] direction in a saddle-shaped 2HTPP molecule on $TiO_2(110)$-1×1 (see Fig. S2 in the ESI† for a comparison).[34] In view of this, a tilted conformation is proposed for the adsorbed two-lobed 2HTPP. In this conformation, two adjacent phenyl groups are in contact with the bottom of trough, while the other two phenyl groups are elevated above the surface, as shown by the DFT calculated adsorption model in Fig. 4c (side and top view). The simulated STM image based on this adsorption configuration is shown in Fig. 4b along with an overlaid molecular model. The appearance of the simulated STM image of a single 2HTPP molecule agrees well with the experimental results in Fig. 4a (marked with white rectangle). Therefore, two bright lobes of 2HTPP are associated with
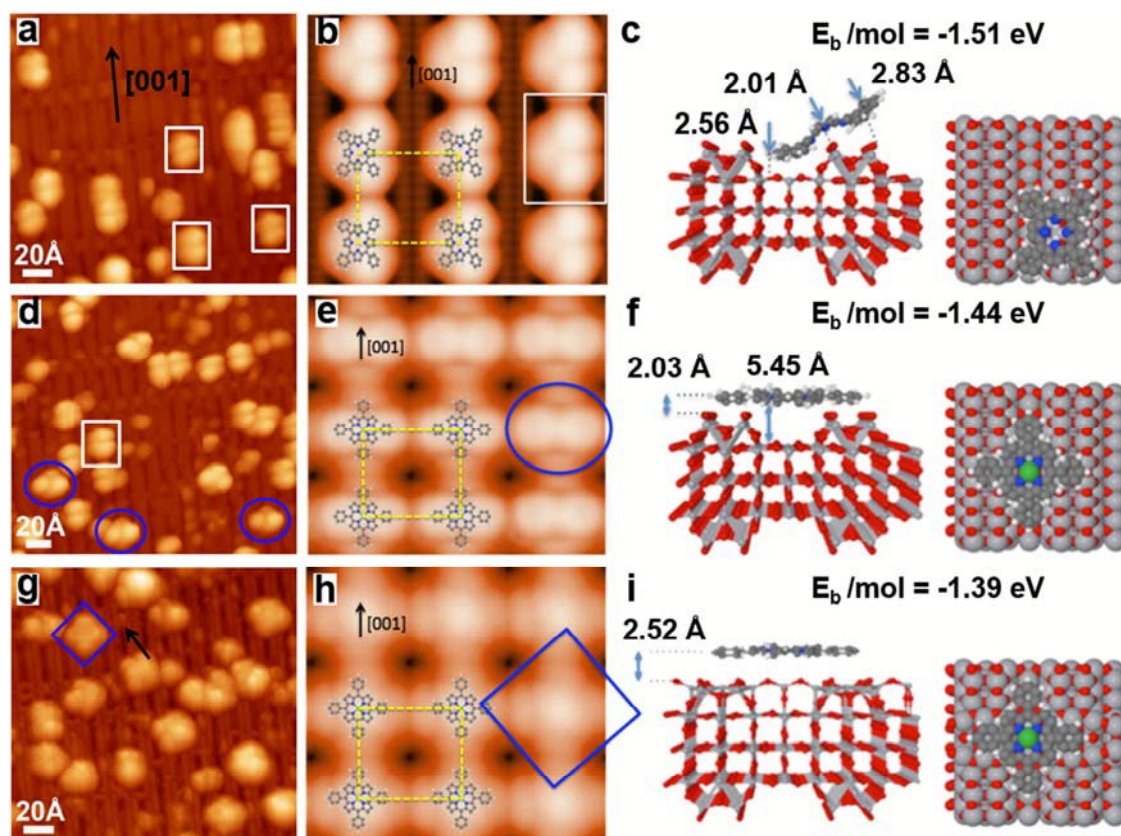
Fig. 4 Comparison between experimental and corresponding DFT-calculated STM images for (a, b) deposition of a 2HTPP submonolayer ($\theta_{2HTPP} = 0.02$) on $TiO_2(110)$-1×2 ; (d, e) incremental deposition of Ni onto 2HTPP with Ni:2HTPP ratios of 1:1; (g, h) heating sample with a 3-fold Ni excess (Ni:2HTPP = 3:1) to 550 K. Three types of molecules are labelled by white rectangle, blue oval and square. The black arrow pointed a CL site. The DFT-calculated STM images are overlaid with molecular models. Optimized side and top view of molecular adsorption models: (c) 2HTPP at added row site, (f) NiTPP atop of a trough and (i) NiTPP at a CL site. For the color code of the substrate atoms, refer to that in Fig. 1c. The gray, white, blue and green balls in 2HTPP and NiTPP represent carbon, hydrogen, nitrogen and Ni atoms. Tunnelling parameters in experiment and calculations: (a, b) I = 0.02 nA; (d, e) I = 0.04 nA; (g, h) I = 0.02 nA; the sample bias voltage was - 2.2 V in all cases. The adsorption energies for the different molecular models are shown on the upper corners of the panel c, f, and i.

two adjacent phenyl rings above the surface. The tilted adsorption conformation may seem unusual and energetically unfavorable, because of the reduced contact area between surface and molecule, but it is not unprecedented: for the structurally related copper phthalocyanine (CuPc) on cross-linked $TiO_2(110)$-1×2, a similar tilted configuration has previously been observed, besides another configuration with the molecular plane parallel to the surface.[61] In addition, an adsorption energy of -1.51 eV per molecule was obtained by our DFT calculations, suggesting that the 2HTPP is stable within the proposed adsorption configuration.

In addition, the 2HTPP molecules on the surface are disordered without assembling into close-packed domains, similar to the behaviour on strongly interacting metal surfaces such as Cu(111), where the disorder was attributed to the localized N-Cu bonds and the formation of dipoles perpendicular to the surface, which result in intermolecular repulsion.[31, 33] In our case of $2HTPP/TiO_2$, hydrogen bonds are proposed to be formed between H atoms in two bottom phenyl groups and oxygen in the surface troughs based on the calculated distance of 2.56 Å between them (Fig. 4c). Additional stabilization results from N-H-O hydrogen bonds between the pyrrolic groups (-NH-) and bridging oxygen atoms in the topmost layer of the Ti_2O_3-added rows (calculated distance 2.01 Å, see Fig. 4c). In contrast to 2HTPP on metal surfaces, where the molecule interacts strongly with the substrate through its iminic N atoms (=N-), a relatively weak interaction is reported here between iminic N atoms and the $TiO_2(110)$-1×2 surface. This is evidenced by the binding energy separation between the pyrrolic and iminic N 1s signals for 2HTPP on $TiO_2(110)$-1×2 of 2.2 eV (Fig. 2a), which is very similar to the value reported for the multilayer (2.1 eV).[62] For comparison, a much smaller separation of only 1.5 eV was reported for 2HTPP on Cu(111).[62] The value for 2HTPP on $TiO_2(110)$-1×1, 1.9 eV, was closer to the value for $TiO_2(110)$-1×2.[34]

Fig. 3c shows the STM image acquired after deposition of the stoichiometric amount of Ni (i.e., one Ni atom per 2HTPP) onto the sample in Fig. 3a at 300 K. Interestingly, after deposition of Ni, molecules with four-lobe feature emerge on the surface (examples are

marked by blue ovals) together with the remaining two-lobed 2HTPP molecules (example marked by white rectangle). The statistical analysis of multiple STM images taken on the same sample as in Fig. 3c shows that the proportion of the four-lobe adsorbates is ~24%, which agrees well with the yield of NiTPP of ~27%, as was calculated from the corresponding XPS data. Thus we assign the observed four-lobe adsorbates to the NiTPP molecules formed by metalation of 2HTPP with Ni. Careful inspection of these four-lobed NiTPP molecules marked by blue ovals reveals that two diagonal lobes along the [001] direction are darker than the other two lobes along the [1$\bar{1}$0] direction. According to previous work, the four lobes are related to the four peripheral phenyl groups of the adsorbed NiTPP.[63] This means that the two diagonal phenyl groups which are oriented along the [001] direction sit at a lower site on $TiO_2(110)$-1×2 than the other two phenyl groups. This adsorption geometry is confirmed by the DFT calculation shown by Fig. 4f: NiTPP adsorbs on $TiO_2(110)$-1×2 with its center located on top of the troughs and is rotated by ~45° relative to 2HTPP. Two diagonal phenyl groups along the [001] direction bend downwards slightly. The other two phenyl groups sit on the Ti_2O_3-added rows, which leads to their increased apparent height relative to the phenyl groups in the troughs. A simulated STM image based on this adsorption structure (Fig. 4e) corresponds well with the experimental STM image in Fig. 4d.

Increasing the amount of deposited Ni to Ni:2HTPP ratios of 2:1 and 3:1 leads to higher metalation degrees of ~36% and ~44%, respectively, as shown in Fig. 3d and 3e. This again agrees with the results from the XP spectra presented above. Fig. 3f shows the STM image taken after heating the sample in Fig. 3e to 550 K. The degree of metalation increased to ~70%, also in agreement with the XPS results. Note that post-annealing of the sample did not result in increased metalation degrees in the case of metalation of 2HTPP with Ni on $TiO_2(110)$-1×1.[34] This difference most likely arises from the fact that the CL and single-link (SL) structures of $TiO_2(110)$-1×2 prevent the growth of large Ni particles, resulting in the formation of more dispersive and smaller Ni particles as mentioned above.[64] This is further confirmed by STM images as discussed below. Noteworthy,
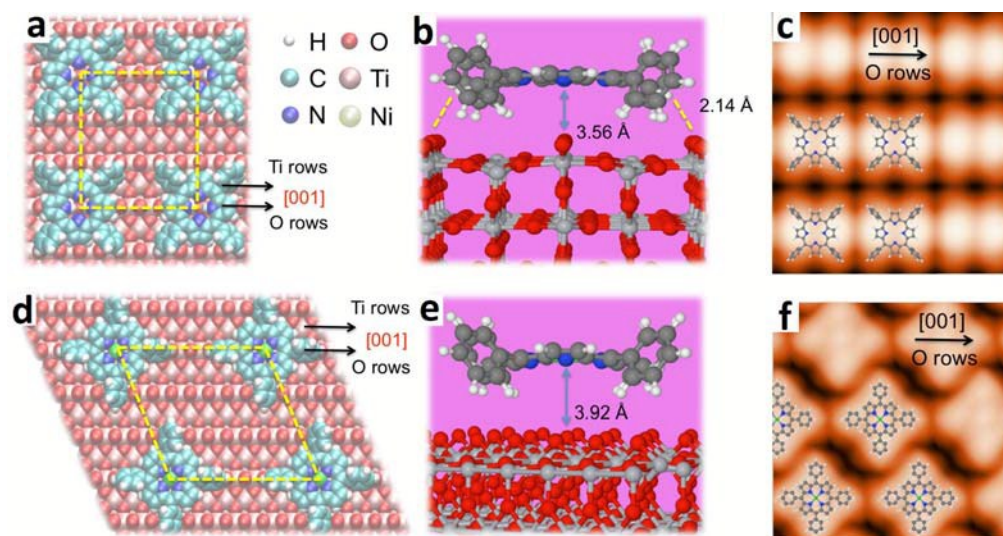

Fig. 5 Optimized adsorption geometries and simulated STM images of 2HTPP and NiTPP on the $TiO_2(110)$-1×1 surface, according to DFT calculations: (a-c) 2HTPP, (d-f) NiTPP.

the NiTPP in Fig. 3f (marked with blue square) shows an almost uniform contrast of four lobes, which indicates that this molecule adsorbs at a different site than those marked by ovals in Fig. 3c. In addition, these NiTPP molecules are typically observed near the CLs, which strongly implies that they are adsorbed on the center of a CL. DFT calculations give the optimal adsorption geometry for NiTPP adsorbed on a CL site as shown in Fig. 4i. NiTPP at a CL site has a "flatter" geometry than NiTPP at the center of the troughs (Fig. 4f). This is manifested by the more uniform four lobes of the simulated STM image for NiTPP adsorbed on CL site, which again agrees with the experimental results as marked by blue rectangle in Fig. 4g. The NiTPP molecules on CLs may be stabilized by the interaction of the central Ni atom with the underlying O atoms in CLs and also by the interaction of the hydrogen atoms in the phenyl groups with the substrate.[61] In conclusion, three types of configuration were observed for the adsorption of 2HTPP and NiTPP on the $TiO_2(110)$-1×2 cross-linked surface.

For comparison, Fig. 5 shows the calculated adsorption geometry of 2HTPP and NiTPP on the $TiO_2(110)$-1×1 surface, along with simulated STM images. The corresponding experimental data were discussed in a previous publication.[34] As can be seen, there are substantial differences between the adsorption structures on $TiO_2(110)$-1×1 and on $TiO_2(110)$-1×2. In the case of $TiO_2(110)$-1×1, both 2HTPP and NiTPP were found to lie with the porphin core plane parallel to the surface, leading to the saddle-shaped configuration of 2HTPP and four-lobed configuration of NiTPP as shown by simulated STM image in Fig. 5c and 5f, respectively, and the previously published experimental STM data.[34] This resembles the configuration of 2HTPP and NiTPP on metal surfaces,[1, 2] although the saddle-shape deformation is much less pronounced. However, on the more corrugated $TiO_2(110)$-1×2 surface, the peripheral phenyl groups interact with the oxygen atoms in the troughs, resulting in a tilted geometry for 2HTPP and a four-lobed feature with two weaker lobes for NiTPP. Only NiTPP molecules adsorbed on CL sites maintain a four-lobed feature because of the relatively flat area on top of a CL.

For comparison with the NiTPP produced by on-surface synthesis, NiTPP was directly deposited onto the $TiO_2(110)$-1×2 surface. Most remarkably, this NiTPP was not found to rotate, but instead had a similar orientation as the 2HTPP molecules. There are many possible reasons for this effect, some of which we discuss in the following. One possibility is the release of the reaction energy during metalation, which may induce the rotational motion. This energy is between 290 and 748 kJ/mol[17] and thus very substantial. Second, the hydrogen atoms released from the -NH- groups during metalation may bind to the oxygen atoms underneath the porphyrin, changing the local surface structure and bonding situation. One may even speculate that changes of the surface electronic structure caused by the presence of the metallic Ni are linked to the observed differences. Due to the complexity of this reactive multi-component adsorbate system, a final conclusion cannot be reached within the scope of this paper.

Reaction of (sub)monolayer 2HTPP with pre-deposited Ni

In the following, metalation using the reverse order of deposition was studied, that is, Ni was pre-deposited onto $TiO_2(110)$-1×2 at 300 K, followed by deposition of a monolayer of 2HTPP. Different from
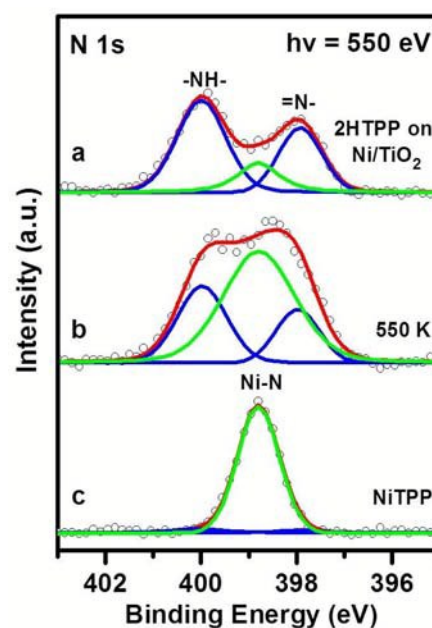

Fig. 6 N 1s XP spectra of (a) a complete 2HTPP monolayer on pre-deposited Ni on $TiO_2(110)$-1×2 at 300 K, θ_{Ni} = 0.197. (b) After heating the sample (a) to 550 K. (c) A complete monolayer of NiTPP on $TiO_2(110)$-1×2 for comparison. The photon energy was 550 eV.

the procedure with Ni post-deposition at room temperature, the N 1s spectrum (Fig. 6a) shows both 2HTPP- and NiTPP-related peaks, indicating that the metalation occurs directly at 300 K with a metalation degree of ~18%, which was also confirmed by valence band spectra, as shown in Fig. S3 (see ESI†). It has been reported that metalation of 2HTPP on the $TiO_2(110)$-1×1 surface with pre-deposited Ni only occurred at elevated temperatures.[34] A possible explanation for this difference is related to the above-mentioned observation that Ni forms smaller clusters on $TiO_2(110)$-1×2 than on $TiO_2(110)$-1×1. The increased surface energy of the smaller clusters results in a higher 2D equilibrium vapor pressure of the Ni atoms, i.e., in a better availability of Ni atoms. However, there may be more complex factors involved: for example, it is likely that Ni atoms can only diffuse inside the troughs on the $TiO_2(110)$-1×1 surface, whereas on $TiO_2(110)$-1×2 additional diffusion on the topmost layers of the Ti_2O_3 rows should be possible. While the Ni atoms in the troughs may be too distant from the porphyrins centers to engage in the metalation reaction, Ni atoms on the Ti_2O_3 rows are closer to the centers of 2HTPP and thus should react more easily at room temperature.

After annealing the inverse-deposition sample to 550 K, the metalation ratio increased to ~49%, as calculated from the spectrum in Fig. 6b. This is less than the maximum metalation degree on $TiO_2(110)$-1×1, which was ~ 60% under otherwise identical conditions.[34] This is an interesting observation, because based on the smaller Ni clusters one would again expect higher metalation degrees on $TiO_2(110)$-1×2, similar to the case when 2HTPP was deposited first. The unexpected result indicates that additional factors play a role here. A possible factor is that the pre-deposited Ni atoms on $TiO_2(110)$-1×2 first aggregate into clusters at sites vicinal to CL or SL, which hinders the diffusion of Ni atoms along troughs even after providing sufficient substrate temperature. This process, however,

cannot happen if 2HTPP molecules are deposited first, since they preferentially occupy these link sites, as shown by STM images in Fig. 3.
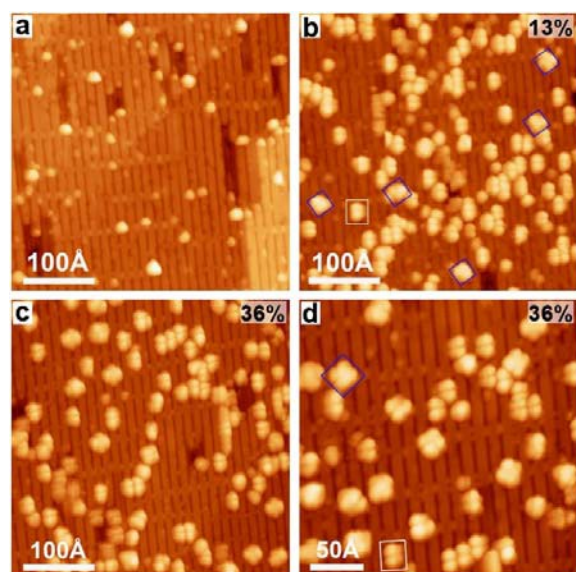
Fig. 7 Constant-current STM images taken after (a) deposition of Ni onto $TiO_2(110)$-1×2, θ_{Ni} = 0.02, (b) deposition of 2HTPP onto Ni/TiO2(110) at 300 K (Ni:2HTPP = 1:1), (c) subsequent heating sample (b) to 550 K, (d) the magnified STM image of the same sample with (c). Two types of molecules are labelled by white rectangle and blue square. Tunnelling parameters: (a) I = 0.07 nA; (b) I = 0.08 nA; (c, d) I = 0.04 nA; in all cases U = - 2.2 V. The average metalation degree (error ± 8%) of 2HTPP is shown on the upper right corners of the panel b-d.

This interpretation is supported by the STM image in Fig. 7a taken after deposition of submonolayer Ni (θ_{Ni} = 0.02) onto $TiO_2(110)$-1×2. The Ni clusters appear on the surface as bright dots with smaller size and higher density located near CL and SL sites compared to $TiO_2(110)$-1×1, as shown by the statistical data in Fig. S4 (ESI†). After vapor deposition of 2HTPP onto the sample shown in Fig. 7a, a small amount of four-lobed rotated molecules (NiTPP) can be found (marked by the blue square in Fig. 7b) with a yield of ~13%. This result indicates that metalation occurs at 300 K and is in fair agreement with the ~18% yield calculated from corresponding XPS data above. Further annealing the sample to 550 K leads to the increase of the metalation degree to ~36%, as shown by the increased number of four-lobed species in Fig. 7c, which is again consistent with the XPS results. Noteworthy, most of the formed NiTPP molecules in Fig. 7d (magnified view of the same sample with Fig. 7c) adsorbed near CLs or SLs with a uniform four-lobed configuration (marked by blue squares), which has been evidenced as NiTPP on CL sites as shown in Fig. 4i. The most likely reason is that the 2HTPP molecules have a tendency to diffuse on the surface and to adsorb on a CL site, to which they bind more strongly than to other sites. Additionally, Ni clusters adsorb stably near the CL sites, making the CL sites more accessible for 2HTPP molecules to pick up Ni atoms released by Ni clusters. Once NiTPP molecules are formed at CL sites, they are stuck there through the interaction of their coordinated Ni ions with oxygen atoms on the CL sites.

Finally, one may ask why only moderate degrees of metalation can be achieved on TiO_2, in stark contrast to metal surfaces, where the reaction proceeds with high yields. Although no final answer can be given on the basis of our data, it appears likely that the interaction between 2HTPP and the TiO_2 surface plays a crucial role, which is not yet fully understood. Some of the 2HTPP molecules may bind so strongly to the substrate with their nitrogen atoms (possible at defect sites) that coordination to a Ni atom is energetically unfavorable. This could also account for the observed differences between $TiO_2(110)$-1×2 and $TiO_2(110)$-1×1. For further clarification, it would be necessary to identify the nature of the adsorption sites beneath the individual 2HTPP molecules, which is a challenging task for further investigations.

Conclusions

We have shown that 2HTPP on $TiO_2(110)$-1×2 reacts with co-adsorbed Ni at room temperature to form the NiTPP complex. The reaction occurs regardless of which reactant is deposited first although with different yields. The metalation from 2HTPP to NiTPP is accompanied by changes of the molecular configuration from a tilted two-lobed feature extending along the [001] direction to a four-lobed feature with two diagonal phenyl groups oriented along the [001] direction. The two phenyl rings oriented along the [001] direction appear darker in the STM images, because they are bent downward into the troughs. When NiTPP is adsorbed on the cross-linked (CL) sites, the four phenyl lobes appear more uniform. This is confirmed by DFT-based STM simulations. Increasing the amount of Ni leads to higher degrees of metalation. The maximum values observed in this work are ~85% with a 3-fold Ni excess and ~49% with 1:1 Ni/2HTPP ratio for 2HTPP reacting with post- and pre-deposited Ni, respectively after annealing to 550 K. Ni clusters are formed with smaller size and higher density at sites vicinal to CL or SL, which enlarged the maximum metalation degree of 2HTPP reacting with post-deposited Ni compared to that on $TiO_2(110)$-1×1. In short, this study shows that the adsorbate-substrate interactions between Ni and/or 2HTPP and different substrates strongly influence the metalation process of 2HTPP. It thus contributes to a better understanding of the direct on-surface metalation of porphyrins and of surface-confined coordination reactions in general.

Acknowledgements

References

1. J. M. Gottfried, *Surf. Sci. Rep.*, 2015, **70**, 259-379.
2. W. Auwärter, D. Écija, F. Klappenberger and J. V. Barth, *Nat. Chem.*, 2015, **7**, 105-120.
3. I. Beletskaya, V. S. Tyurin, A. Y. Tsivadze, R. Guilard and C. Stern, *Chem. Rev.*, 2009, **109**, 1659-1713.
4. D. Bonifazi, A. Kiebele, M. Stöhr, F. Cheng, T. Jung, F. Diederich and H. Spillmann, *Adv. Funct. Mater.*, 2007, **17**, 1051-1062.
5. C. M. Drain, A. Varotto and I. Radivojevic, *Chem. Rev.*, 2009, **109**, 1630-1658.
6. C. Wäckerlin, K. Tarafder, D. Siewert, J. Girovsky, T. Hählen, C. Iacovita, A. Kleibert, F. Nolting, T. A. Jung, P. M. Oppeneer and N. Ballav, *Chem. Sci.*, 2012, **3**, 3154-3160.
7. J. Kim, S.-H. Lim, Y. Yoon, T. D. Thangadurai and S. Yoon, *Tetrahedron Lett.*, 2011, **52**, 2645-2648.
8. D. P. Arnold, D. Manno, G. Micocci, A. Serra, A. Tepore and L. Valli, *Thin Solid Films*, 1998, **327-329**, 341-344.
9. L. Wang, H. Li, J. Deng and D. Cao, *Curr. Org. Chem.*, 2013, **17**, 3078-3091.
10. A. Tepore, A. Serra, D. Manno, L. Valli, G. Micocci and D. P. Arnold, *J. Appl. Phys.*, 1998, **84**, 1416-1420.
11. N. A. Rakow and K. S. Suslick, *Nature*, 2000, **406**, 710-713.
12. M. Marin-Suárez, S. Medina-Rodríguez, O. Ergeneman, S. Pané , J. F. Fernández-Sánchez, B. J. Nelson and A. Fernández-Gutiérrez, *Nanoscale*, 2014, **6**, 263-271.
13. I. Mochida, K. Suetsugu, H. Fujitsu and K. Takeshita, *J. Phys. Chem.*, 1983, **87**, 1524-1529.
14. Y. Zhong, J. Wang, R. Zhang, W. Wei, H. Wang, X. Lü, F. Bai, H. Wu, R. Haddad and H. Fan, *Nano Lett.*, 2014, **14**, 7175-7179.
15. A. Trojánek, J. Langmaier, H. Kvapilová, S. Záliš and Z. Samec, *J. Phys. Chem. A*, 2014, **118**, 2018-2028.
16. J. M. Gottfried, K. Flechtner, A. Kretschmann, T. Lukasczyk and H.-P. Steinrück, *J. Am. Chem. Soc.*, 2006, **128**, 5644-5645.
17. T. E. Shubina, H. Marbach, K. Flechtner, A. Kretschmann, N. Jux, F. Buchner, H.-P. Steinrück, T. Clark and J. M. Gottfried, *J. Am. Chem. Soc.*, 2007, **129**, 9476-9483.
18. W. Auwärter, A. Weber-Bargioni, S. Brink, A. Riemann, A. Schiffrin, M. Ruben and J. V. Barth, *ChemPhysChem*, 2007, **8**, 250-254.
19. F. Buchner, K. Flechtner, Y. Bai, E. Zillner, I. Kellner, H.-P. Steinrück, H. Marbach and J. M. Gottfried, *J. Phys. Chem. C*, 2008, **112**, 15458-15465.
20. F. Buchner, K.-G. Warnick, T. Wölfle, A. Görling, H.-P. Steinrück, W. Hieringer and H. Marbach, *J. Phys. Chem. C*, 2009, **113**, 16450-16457.
21. F. Buchner, V. Schwald, K. Comanici, H.-P. Steinrück and H. Marbach, *ChemPhysChem*, 2007, **8**, 241-243.
22. D. Écija, W. Auwärter, S. Vijayaraghavan, K. Seufert, F. Bischoff, K. Tashiro and J. V. Barth, *Angew. Chem., Int. Ed.*, 2011, **50**, 3872-3877.
23. K. Flechtner, A. Kretschmann, L. R. Bradshaw, M.-M. Walz, H.-P. Steinrück and J. M. Gottfried, *J. Phys. Chem. C*, 2007, **111**, 5821-5824.
24. A. Kretschmann, M.-M. Walz, K. Flechtner, H.-P. Steinrück and J. M. Gottfried, *Chem. Commun.*, 2007, 568-570.
25. A. Weber-Bargioni, J. Reichert, A. P. Seitsonen, W. Auwärter, A. Schiffrin and J. V. Barth, *J. Phys. Chem. C*, 2008, **112**, 3453-3455.
26. M. Chen, X. Feng, L. Zhang, H. Ju, Q. Xu, J. Zhu, J. M. Gottfried, K. Ibrahim, H. Qian and J. Wang, *J. Phys. Chem. C*, 2010, **114**, 9908-9916.

27. F. Buchner, I. Kellner, H.-P. Steinrück and H. Marbach, *Z. Phys. Chem.*, 2009, **223**, 131-144.
28. K. Diller, F. Klappenberger, M. Marschall, K. Hermann, A. Nefedov, C. Wöll and J. V. Barth, *J. Chem. Phys.*, 2012, **136**, 014705.
29. S. Ditze, M. Stark, M. Drost, F. Buchner, H.-P. Steinrück and H. Marbach, *Angew. Chem., Int. Ed.*, 2012, **51**, 10898-10901.
30. A. Goldoni, C. A. Pignedoli, G. Di Santo, C. Castellarin-Cudia, E. Magnano, F. Bondino, A. Verdini and D. Passerone, *ACS Nano*, 2012, **6**, 10800-10807.
31. M. Stark, S. Ditze, M. Drost, F. Buchner, H.-P. Steinrück and H. Marbach, *Langmuir*, 2013, **29**, 4104-4110.
32. J. Nowakowski, C. Wäckerlin, J. Girovsky, D. Siewert, T. A. Jung and N. Ballav, *Chem. Commun.*, 2013, **49**, 2347-2349.
33. J. Xiao, S. Ditze, M. Chen, F. Buchner, M. Stark, M. Drost, H.-P. Steinrück, J. M. Gottfried and H. Marbach, *J. Phys. Chem. C*, 2012, **116**, 12275-12282.
34. C. Wang, Q. Fan, S. Hu, H. Ju, X. Feng, Y. Han, H. Pan, J. Zhu and J. M. Gottfried, *Chem. Commun.*, 2014, **50**, 8291-8294.
35. W. M. Campbell, A. K. Burrell, D. L. Officer and K. W. Jolley, *Coord. Chem. Rev.*, 2004, **248**, 1363-1379.
36. M. K. Nazeeruddin, R. Humphry-Baker, D. L. Officer, W. M. Campbell, A. K. Burrell and M. Grätzel, *Langmuir*, 2004, **20**, 6514-6517.
37. L. Schmidt-Mende, W. M. Campbell, Q. Wang, K. W. Jolley, D. L. Officer, M. K. Nazeeruddin and M. Grätzel, *ChemPhysChem*, 2005, **6**, 1253-1258.
38. Y. Tachibana, S. A. Haque, I. P. Mercer, J. R. Durrant and D. R. Klug, *J. Phys. Chem. B*, 2000, **104**, 1198-1205.
39. I. Mochida, K. Tsuji, K. Suetsugu, H. Fujitsu and K. Takeshita, *J. Phys. Chem.*, 1980, **84**, 3159-3162.
40. I. Mochida, K. Suetsugu, H. Fujitsu, K. Takeshita, K. Tsuji, Y. Sagara and A. Ohyoshi, *J. Catal.*, 1982, **77**, 519-526.
41. D. Chen, D. Yang, J. Geng, J. Zhu and Z. Jiang, *Appl. Surf. Sci.*, 2008, **255**, 2879-2884.
42. J. Niu, B. Yao, Y. Chen, C. Peng, X. Yu, J. Zhang and G. Bai, *Appl. Surf. Sci.*, 2013, **271**, 39-44.
43. U. Diebold, *Surf. Sci. Rep.*, 2003, **48**, 53-229.
44. I. Horcas, R. Fernández, J. M. Gómez-Rodriguez, J. Colchero, J. Gómez-Herrero and A. M. Baro, *Rev. Sci. Instrum.*, 2007, **78**, 013705.
45. J. P. Lewis, P. Jelínek, J. Ortega, A. A. Demkov, D. G. Trabada, B. Haycock, H. Wang, G. Adams, J. K. Tomfohr, E. Abad, H. Wang and D. A. Drabold, *Phys. Stat. Sol. B*, 2011, **248**, 1989-2007.
46. P. Giannozzi, S. Baroni, N. Bonini, M. Calandra, R. Car, C. Cavazzoni, D. Ceresoli, G. L. Chiarotti, M. Cococcioni, I. Dabo, A. Dal Corso, S. de Gironcoli, S. Fabris, G. Fratesi, R. Gebauer, U. Gerstmann, C. Gougoussis, A. Kokalj, M. Lazzeri, L. Martin-Samos, N. Marzari, F. Mauri, R. Mazzarello, S. Paolini, A. Pasquarello, L. Paulatto, C. Sbraccia, S. Scandolo, G. Sclauzero, A. P. Seitsonen, A. Smogunov, P. Umari and R. M. Wentzcovitch, *J. Phys.: Condens. Matter*, 2009, **21**, 395502.
47. S. Grimme, *J. Comp. Chem.*, 2006, **27**, 1787-1799.
48. J. M. Blanco, C. González, P. Jelínek, J. Ortega, F. Flores and R. Pérez, *Phys. Rev. B*, 2004, **70**, 085405.
49. T. Bredow, L. Giordano, F. Cinquini and G. Pacchioni, *Phys. Rev. B*, 2004, **70**, 035419.
50. H. Onishi and Y. Iwasawa, *Surf. Sci.*, 1994, **313**, L783-L789.
51. H. Onishi and Y. Iwasawa, *Phys. Rev. Lett.*, 1996, **76**, 791-794.
52. P. Krüger, S. Bourgeois, B. Domenichini, H. Magnan, D. Chandesris, P. Le Fèvre, A. M. Flank, J. Jupille, L. Floreano, A. Cossaro, A. Verdini and A. Morgante, *Phys. Rev. Lett*, 2008, **100**, 055501.
53. K. T. Park, M. H. Pan, V. Meunier and E. W. Plummer, *Phys. Rev. Lett.*, 2006, **96**, 226105.
54. N. Shibata, A. Goto, S . -Y. Choi, T. Mizoguchi, S. D. Findlay, T. Yamamoto and Y. Ikuhara, *Science*, 2008, **322**, 570-573.

55. S. D. Elliott and S. P. Bates, *Phys. Rev. B*, 2003, **67**, 035421.
56. H. Ünal, E. Mete and S. Ellialtıoğlu, *Phys. Rev. B*, 2011, **84**, 115407.
57. S. Takakusagi, K.-i. Fukui, F. Nariyuki and Y. Iwasawa, *Surf. Sci.*, 2003, **523**, L41-L46.
58. P. Stone, R. A. Bennett and M. Bowker, *New J. Phys*, 1999, **1**, 1.1-1.12.
59. D. A. Chen, New Catalysts *for the Destruction of Chemical Warfare Agents*. *DTIC Document*, 2005.
60. W. Auwärter, F. Klappenberger, A. Weber-Bargioni, A. Schiffrin, T. Strunskus, C. Wöll, Y. Pennec, A. Riemann and J. V. Barth, *J. Am. Chem. Soc.*, 2007, **129**, 11279-11285.
61. Y. Wang, Y. Ye and K. Wu, *J. Phys. Chem. B*, 2006, **110**, 17960-17965.
62. F. Buchner, J. Xiao, E. Zillner, M. Chen, M. Röckert, S. Ditze, M. Stark, H.-P. Steinrück, J. M. Gottfried and H. Marbach, *J. Phys. Chem. C*, 2011, **115**, 24172-24177.
63. L. G. Teugels, L. G. Avila-Bront and S. J. Sibener, *J. Phys. Chem. C*, 2011, **115**, 2826-2834.
64. Y. Maeda, T. Fujitani, S. Tsubota and M. Haruta, *Surf. Sci.*, 2004, **562**, 1-6.